Effects of axial boundary conductivity on a free Stewartson-Shercliff layer

Kyle J. Caspary,[1,*] Dahan Choi,[2] Fatima Ebrahimi,[1] Erik P. Gilson,[1] Jeremy Goodman,[2] and Hantao Ji[1,2]

[1]*Princeton Plasma Physics Laboratory, Princeton University, Princeton, New Jersey 08543, USA*
[2]*Department of Astrophysical Sciences, Princeton University, Princeton, New Jersey 08540, USA*

The effects of axial boundary conductivity on the formation and stability of a magnetized free Stewartson-Shercliff layer (SSL) in a short Taylor-Couette device are reported. As the axial field increases with insulating endcaps, hydrodynamic Kelvin-Helmholtz-type instabilities set in at the SSLs of the conducting fluid, resulting in a much reduced flow shear. With conducting endcaps, SSLs respond to an axial field weaker by the square root of the conductivity ratio of endcaps to fluid. Flow shear continuously builds up as the axial field increases despite the local violation of the Rayleigh criterion, leading to a large number of hydrodynamically unstable modes. Numerical simulations of both the mean flow and the instabilities are in agreement with the experimental results.

I. INTRODUCTION

The importance of boundaries is widely known for liquid, gas, and plasma systems in fluid dynamics and plasma physics, as well as in geophysics and astrophysics. The importance lies not only with the formation of boundary layers but also with their impact on the bulk flow. For rotating flows, Ekman [1] and Stewartson [2] layers form on surfaces perpendicular and parallel to the rotation axis, respectively, inducing secondary circulations, and significantly altering bulk flows and stability. A vivid example of the latter was shown in previous experiments [3,4] aimed at studying the hydrodynamic stability of quasi-Keplerian flows relevant to accretion disk stability in astrophysics [5].

For electrically conducting fluids in the presence of an applied magnetic field, induced currents can substantially alter the flow. In addition to secondary flow circulation, there is an induced Hartmann current that closes through Hartmann [6] and Shercliff [7] layers formed on surfaces perpendicular and parallel to the external field, respectively. Clearly, the conductivity of the boundaries is important as the induced current is larger within boundaries that are more conductive (see, e.g., Ref. [8]).

Gilman and others [9–12] analyzed Ekman-Hartmann layers forming on endcap surfaces perpendicular to both the rotation axis and the axial field due to combined rotation and fluid conductivity effects. Complementary Stewartson-Shercliff layers (SSLs) form on surfaces parallel to the rotation axis and axial field. However, when the endcaps include a pair of differentially rotating rings, a free SSL can form within the conducting fluid exhibiting a hydrodynamic Kelvin-Helmholtz-type instability when the magnetic field or shear is sufficiently strong [13,14].

Boundary effects play an important role in laboratory searches for the magnetorotational instability (MRI), which is probably the dominant source of turbulence in astronomical accretion disks [15]. MRI requires differential rotation within a magnetized conducting fluid. In contrast to gravitationally driven accretion disks, terrestrial laboratory flows are usually driven by rotating boundaries in which SSLs are almost unavoidable. Indeed, the first experimental data claimed as evidence for MRI [16] probably had more to do with SSL than MRI [17]. Furthermore, to drive the flow effectively, boundaries must be well coupled to the fluid. At the low magnetic Prandtl numbers characteristic of liquid metals ($\mathrm{Pr}_m \equiv \nu/\eta \lesssim 10^{-5}$), viscous coupling is weak, yielding a low saturation amplitude for nonlinear MRI modes [18]. This serves to motivate the exploration of conducting boundaries with strong coupling to the fluid. Simulations including conducting boundaries show promise [19], but reliable simulations at realistic Pr_m are not presently possible, so experimental studies of SSLs are an essential preliminary step towards carrying out experiments demonstrating MRI.

In this paper, the effects of axial boundary conductivity on the formation and stability of a free SSL are studied. The conducting fluid couples more readily, and at weaker axial fields, to conducting than to insulating endcaps. Larger mean shear develops within the fluid volume despite numerous centrifugal-type hydrodynamic instabilities. Numerical simulations of both the mean flow and the instabilities agree with the experimental results.

II. EXPERIMENTAL SETUP

The Princeton MRI experiment is a modified Taylor-Couette device consisting of two coaxial cylinders with two sets of axial endcap rings (Fig. 1). The device was recently redesigned to further minimize boundary effects and improve the magnetic coupling. Rotating seals were improved, insulating acrylic endcaps were replaced by conducting copper ones, and a 1-cm-wide rim was added to the inner cylinder. These modifications were based in part on the design of a similar apparatus that produces hydrodynamically stable, quasi-Keplerian, sheared flows [4]. The working fluid, a GaInSn eutectic alloy [67% Ga, 20.5% In, 12.5% Sn—
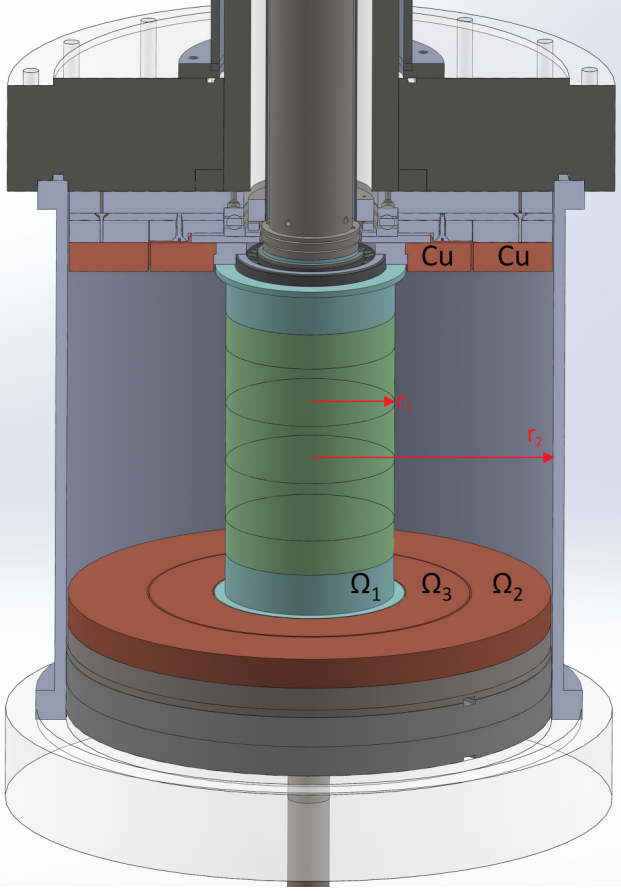
---

*kcaspary@pppl.gov; http://mri.pppl.gov

FIG. 1. Schematic of the redesigned Princeton MRI experiment with three independently rotating components; the inner cylinder with rim (Ω_1), outer cylinder with ring (Ω_2), and inner ring (Ω_3).

FIG. 2. Measurements of the azimuthal velocity at $r = 15.0$ cm for experiments with insulating (a) and conducting (b) endcaps. Measurements are at the midplane for a configuration with $\Omega_1/\Omega_2 = 335$ rpm/100 rpm and $B_z = 4200$ G. In (c) and (d) are spectrograms of the velocity fluctuations for the data shown in (a) and (b), respectively. The field is on during the interval bounded by dashed vertical lines.

$\rho_{\text{Ga}} = 6.3$ g/cm^3, $\sigma_{\text{Ga}} = 3.5 \times 10^6$ (Ωm)$^{-1}$], is liquid at room temperature. The fluid volume has inner radius of $r_1 = 6.9$ cm, outer radius of $r_2 = 20.3$ cm, and height of 28 cm. The inner cylinder, rotating at Ω_1, is made up of several modular components, including stainless steel caps that compress a stack of thick Delrin rings housing diagnostics. The outer cylinder, rotating at Ω_2, is made of stainless steel. Each endcap is split into two rings fabricated out of 1-inch-thick silver-plated copper [$\rho_{\text{Cu}} = 9.0$ g/cm^3, $\sigma_{\text{Cu}} = 6.0 \times 10^7$ (Ωm)$^{-1}$]. The outer endcap ring extends to $r = 13.5$ cm and is bound to the outer cylinder wall, thus also rotating at Ω_2. The inner endcap ring rotates independently at Ω_3 and spans from $r = 8$ cm to $r = 13.5$ cm. Differential rotation of the boundaries can establish a variety of sheared flow profiles $\Omega(r)$, including profiles approaching the ideal Taylor-Couette solution [4] for infinite cylinders, where the angular velocity is $\Omega(r) = a + b/r^2$, with $a = (\Omega_2 r_2^2 - \Omega_1 r_1^2)/(r_2^2 - r_1^2)$ and $b = r_1^2 r_2^2 (\Omega_1 - \Omega_2)/(r_2^2 - r_1^2)$.

The results reported here utilize a "split" configuration where the inner and outer rings spin with the inner and outer cylinders, respectively, resulting in two rotation rates, $\Omega_1(=\Omega_3)$ and Ω_2. Experimental results are compared and contrasted to isolate the effect of the endcap conductivity since the "split" configuration has been used previously [13,14] with insulating endcaps. To establish a stable hydrodynamic flow,
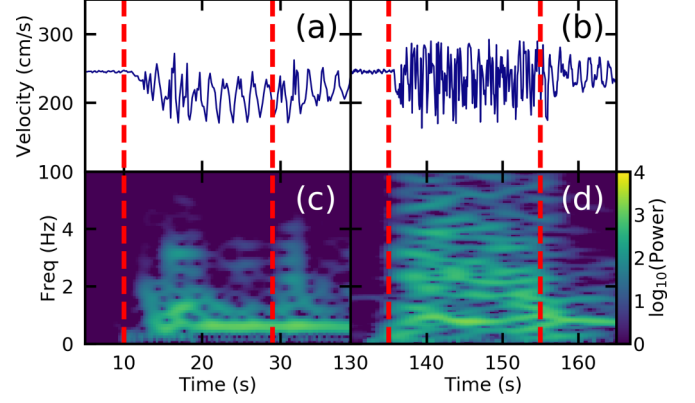
the experiment spins for at least 2 min (several Ekman times) prior to the application of an axial magnetic field of up to $B_z = 4800$ G, provided by a set of six water-cooled coils. The field is applied for 30 s or less to maintain acceptable coil temperatures. The primary diagnostic used in these experiments is a suite of ultrasound Doppler velocimetry (UDV) transducers mounted on the outer cylinder of the experiment [20]. The transducers are aligned along the chords tangent to the inner cylinder. The data discussed are taken at the midplane. Mode information is obtained from the relative phase of identically aligned transducers separated azimuthally by an angle of 90°.

III. RESULTS AND DISCUSSION

Experimental results using endcaps with different conductivities exhibit differences in the time evolution of the measured azimuthal velocity. Figures 2(a) and 2(b) shows azimuthal velocity measurements at $r = 15$ cm for experiments with $B_z = 4200$ G and $\Omega_1/\Omega_2 = 335$ rpm/100 rpm. The flow with conducting endcaps responds more rapidly than with insulating endcaps, within 1 s of applying B_z. The torque exerted on the fluid by insulating endcaps is due only to viscous stress, even with an applied B_z, whereas magnetic stresses dominate the torque with conducting endcaps. In order to estimate their relative strength, a linear boundary layer analysis similar to that in Ref. [9] has been performed to calculate the ratio of magnetic to viscous stresses on the endcaps, with the result that:

$$\frac{F_{\text{mag}}}{F_{\text{visc}}} = \frac{\Lambda_{\text{Ga}}\sqrt{2}}{\sqrt[4]{\Lambda_{\text{Ga}}^2 + 1}} \sqrt{\frac{\Omega_1 L^2}{\nu}}, \quad (1)$$

where $\Lambda_{\text{Ga}} = B_z^2/(\mu_0 \rho_{\text{Ga}} \eta_{\text{Ga}} \Delta\Omega)$ is an Elsasser number based on the fluid's magnetic diffusivity [$\eta_{\text{Ga}} = (\mu_0 \sigma_{\text{Ga}})^{-1}$] and density ($\rho_{\text{Ga}}$) with the difference in angular velocity between endcap rings ($\Delta\Omega$). The effective electrical thickness $L = \sigma_e d_e/\sigma_{\text{Ga}}$, is the geometrical thickness of the endcap, d_e, multiplied by the ratio of endcap and fluid conductivities. One expects this stress ratio to be reflected in the time responses to the applied field for the flow to form a free SSL. Fitting
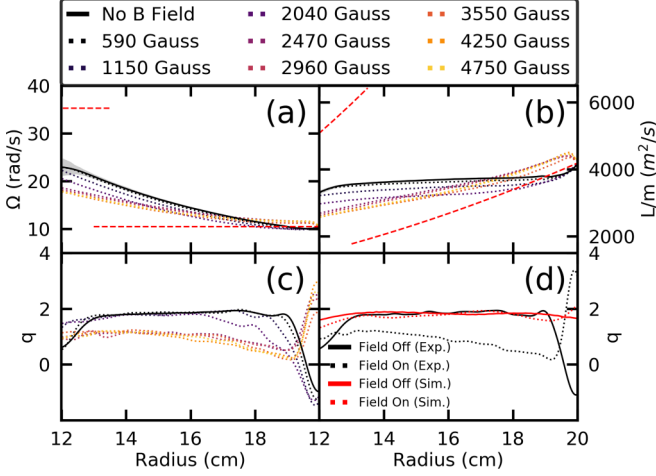
FIG. 3. The time averaged mean angular velocity (a), specific angular momentum (b), and flow shear q profiles (c) before (solid) and during (dotted) the application of a magnetic field over a range of field strengths with insulating endcaps. Shown in (d) is a comparison with simulation for q profiles with and without applied field of 4200 G. All data are averaged over 10 s. The red dashed line corresponds to the boundary rotation of the endcaps at the indicated radius. The gray bands indicate the variance of the time average with no magnetic field and are indicative of the measurement error.

an exponential to the velocity response to applied B_z shown in Fig. 2 yields timescales of 10 s and 0.5 s for the insulating and conducting cases, respectively. However, evaluation of the ratio in Eq. (1) gives $F_{mag}/F_{visc} \sim 5000$ for the parameters of the experimental runs shown in Fig. 2. The difference is likely due to the finite rise time (≈ 1 s) of the coil current (and associated B_z), which is comparable to the timescale observed with conducting endcaps.

Fluctuations develop for the cases of insulating and conducting endcaps but with distinctly different characteristics. With insulating endcaps, a coherent fluctuation saturates 5–10 s after B_z is applied and the mean flow changes concurrently. As $\Lambda_{Ga} > 1$ in this case, Kelvin-Helmholtz-type modes are expected [13]. The conducting endcap case shows a rapid development of high-frequency fluctuations. A spectrogram of the velocity fluctuations [Figs. 2(c) and 2(d)] shows, for insulating endcaps, a higher-frequency fluctuation transitioning to a lower-frequency mode with an apparent azimuthal mode number $m = 1$. In contrast, experiments with conducting endcaps show a complicated mode structure with many simultaneous fluctuations, which are due to Rayleigh unstable, centrifugal-type instabilities (see below).

Not only is the response time more rapid with conducting rather than insulating endcaps, but the resultant flow profiles also differ significantly. Figures 3(a) and 3(b) and then 4(a) and 4(b) show the mean angular velocity and specific angular momentum profiles as B_z changes for experiments with $\Omega_1/\Omega_2 = 335/100$. As B_z increases up to 2040 G in Fig. 3, the angular velocity decreases at all radii. Above 2100 G, when $\Lambda_{Ga} > 1$, the flow is unstable (see Fig. 5 below), resulting in a flattened mean flow profile. In Fig. 4, with conducting endcaps, the angular velocity decreases in the outer region as the B_z increases. For $B_z > 600$ G (see Fig. 5 below), the flow becomes
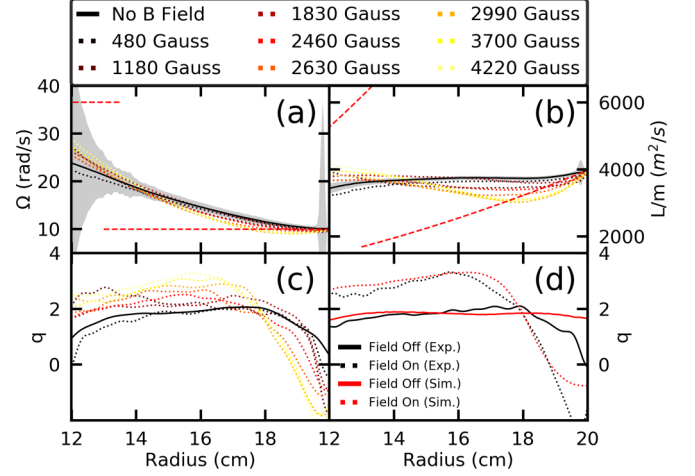

FIG. 4. Same as in Fig. 3 but for conducting endcaps.

unstable due to the increased flow shear. The shear increases substantially as B_z exceeds 2100 G (the stability threshold for insulating endcaps). The instability corresponds to a region of negative slope for the angular momentum profile.

The B_z dependence of the free SSL shear, defined as $q = -d \ln \Omega / d \ln r$, is shown in Figs. 3(c) and 4(c). In the insulating endcap case, q changes little until the onset of the instability in the SSL above $\Lambda_{Ga} = 1$, beyond which q decreases dramatically to $q \sim 1$. The conducting endcap experiments show a significant change in q as B_z increases. For $r < 17.5$ cm, $q > 2$, suggesting that the observed instabilities are Rayleigh unstable centrifugal modes. Interestingly, the peak q values of the free SSL continuously increase despite the presence of instabilities, in sharp contrast to the insulating endcap case.

The evolution of the shear q and the fluctuations as B_z increases are shown in Fig. 5 for both insulating and conducting endcaps. Both q and fluctuating power are averaged over radii from 15.5 to 16.5 cm. For insulating endcap experiments, the flow remains stable until $\Lambda_{Ga} > 1$ where the fluctuating power
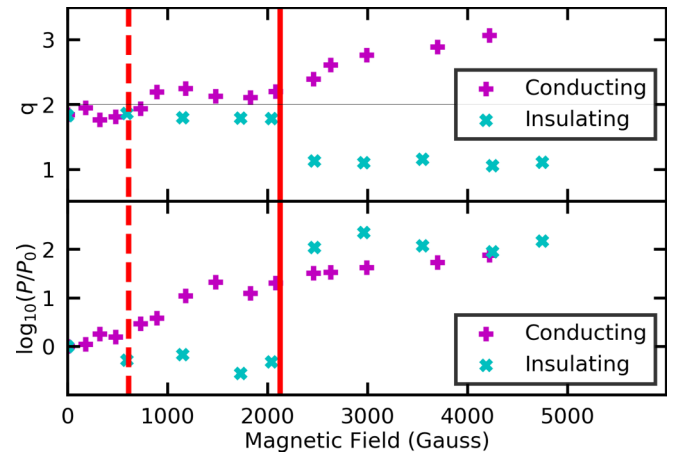

FIG. 5. The average q value (top) and the log of the change in total fluctuating power (bottom) at $r = 16.0$ cm vs. magnetic field comparing experiments with insulating and conducting endcaps. Vertical lines indicate $\Lambda_{Ga} = 1$ (solid) and $\Lambda_{Cu} = 1$ (dashed).

saturates and the average q drops to near 1. Experiments with conducting endcaps begin to show an increase in fluctuations well below $\Lambda_{Ga} = 1$. By changing the density and conductivity in the Elsasser number definition to those of the copper endcaps, a lower threshold Λ_{Cu}, with $\Lambda_{Ga}/\Lambda_{Cu} = 3.5$, appears to be more appropriate. Above $\Lambda_{Cu} = 1$, the average q increases above 2. As the magnetic field continues to increase so that $\Lambda_{Ga} > 1$, q rises above 3. Despite the substantial fluctuating power, the shear layer is maintained by the coupling to the conducting boundary, leading to a flow profile that is in a regime hydrodynamicaly unstable to Rayleigh modes.

Numerical simulations of the experiments have been carried out using the spectral finite element Maxwell and Navier Stokes code [21]. This code is capable of replicating the fluid boundary conditions imposed by the split endcap configuration with both insulating and conducting endcap material in three dimensions [19]. All simulations were performed with a Reynolds number (Re $= \Omega_1 r_1^2/\nu$) of 1000, which is less than experimental values of up to 10^6, due to limited numerical resources. All other aspects of the experiment are modeled as accurately as possible including the endcap thickness and conductivity. The initially stable hydrodynamical free SSLs, or more precisely free Stewartson layers in this case, are realized by choosing the Rossby number, Ro $= (\Omega_1 - \Omega_2)/\Omega_2 = 2.7$–3.0, higher than their experimental values of 2.35–2.4 [14]. The simulations were continued with an applied B_z.

Figures 3(d) and 4(d) compare $q(r)$ with and without an applied axial field for the experiment and simulation. The experimental profiles are the same as discussed above while the simulation profiles are spatial and time averages over five time steps (~ 0.14 s). Despite large differences in Re between the simulations and the experiments, the hydrodynamic profiles are reproduced except at the radial edge where viscosity becomes important. With conducting endcaps, after B_z is applied, the comparison shows a similar q profile away from the viscous boundary layer, indicating that the strong magnetic coupling is reproduced numerically. However, this agreement is absent in the case of insulating endcaps where only viscous coupling exists. This is not surprising given the three orders of magnitude difference in Re between experiment and simulation, and the details are to be explored in the future.

The qualitative agreement with simulation in the case of conducting endcaps gives confidence when drawing additional insights into the mechanisms involved in establishing the free SSL. The simulations show a significantly stronger response to B_z in the conducting endcap case. Figure 6 compares simulations for different boundary conditions showing strong radial currents in the thick conducting endcaps, contrasting with thin boundary layers in the insulating endcap case. This also leads to larger return currents in the fluid and a stronger azimuthal force which reinforces the shear layer. Radial currents result in a torque on the conducting endcaps and, while we lack a quantitative torque measurement, qualitatively, a reduced output is observed in the outer component motors while the field is on in this sheared flow configuration. The continuous increase in q with B_z is also reproduced in simulations with conducting endcaps despite the presence of vigorous instabilities which are presumably driven by the flow shear. This implies that the instabilities are incapable of depleting the free energy in the flow shear that is supplied through the
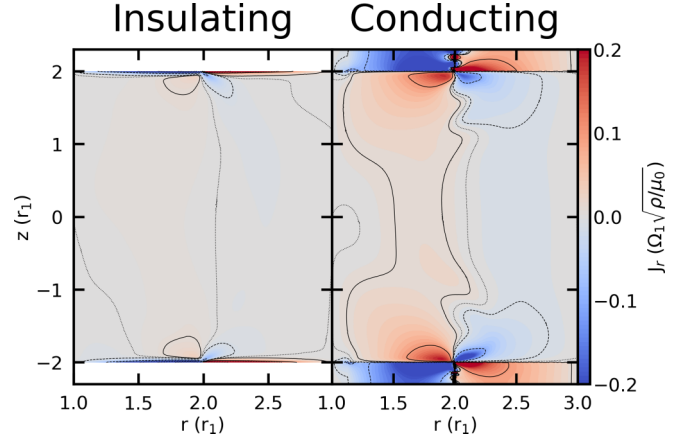

FIG. 6. Contour plot of the normalized radial current for the full device simulations with insulating (left) and conducting (right) endcaps shortly after a magnetic field is applied. The boundary currents remain consistent, but thin current layers in the insulating case are replaced with thick currents in the endcaps, resulting in larger return currents in the fluid. Solid (dashed) contours indicating inward (outward) normalized currents of $+/- 0.1$ and $+/- 0.01$. The dotted contour follows $J_r = 0$.

strong magnetic coupling from the conducting endcaps. This is in sharp contrast to the insulating endcap case, where q spontaneously decreases when instabilities appear, as shown in Fig. 3. This understanding confirms the original motivation [19] to replace insulating endcaps with conducting ones to maintain large flow shear in order to substantially increase the MRI amplitudes through strong magnetic couplings.

The flow that is established with a strong magnetic field is hydrodynamically unstable, as evidenced by the measured flow in Fig. 2 after the field is turned off. When the applied magnetic field ends, a Kelvin-Helmholtz-like instability is observed with $m = 1$ structure. In the insulating case, the Kelvin-Helmholtz mode persists after the field ends at $t = 30$ s. When the field is turned off at $t = 155$ s in the conducting case, a similar hydrodynamic instability manifests as the spectrogram is dominated by a single-frequency fluctuation. The multitude of higher-frequency fluctuations while the field is applied are likely a result of Rayleigh unstable flows due to the sheared profile with $q > 2$. It is possible that the Kelvin-Helmholtz mode is stabilized by line tying effects while the field is applied [22].

IV. CONCLUSIONS

The results presented here describe the effect of the conductivity of the endcap-boundary material on a free Stewartson-Shercliff-layer and the subsequent hydrodynamic instabilities that develop. With conductive endcaps, the shear layer forms at much lower fields and the resulting instability appears to be the result of Rayleigh modes instead of the Kelvin-Helmholtz modes observed with insulating boundaries. Current flowing in the endcaps or in the boundary layer contributes to the increased coupling of the fluid flow to the boundaries. With insulating endcaps, this boundary layer was thin and return currents remain small. With the conducting endcaps, there is a thick boundary layer with significantly lower resistance,

leading to a much stronger current and in turn increased magnetic coupling via return currents in the fluid. This coupling is predicted to increase the observable MRI signal, but also results in a decrease in the stability threshold of the free SSL against Rayleigh-type centrifugal instabilities, which are a focus for future research. Care must be taken not to confuse the two instability mechanisms when interpreting experimental data and future work will aim to establish MHD-stable flows when an axial field is applied to destabilize the MRI. In the present work, the rotation of the inner endcap ring has been chosen to maximize the SSL; when searching for MRI, we will seek to minimize these layers. It has already been shown that the free SSL instability threshold can be increased by altering the boundary conditions such that the flow is optimized to reduce secondary flow prior to the application of magnetic field.

Digital data associated with this work are available from DataSpace at Princeton University [23].

ACKNOWLEDGMENTS

[1] V. W. Ekman, Arch. Math. Astron. Phys. **2**, 1 (1905).

[2] K. Stewartson, J. Fluid Mech. **3**, 17 (1957).

[3] H. Ji, M. Burin, E. Schartman, and J. Goodman, Nature **444**, 343 (2006).

[4] E. M. Edlund and H. Ji, Phys. Rev. E **89**, 021004 (2014).

[5] H. Ji and S. Balbus, Phys. Today **66**, 27 (2013).

[6] J. Hartmann, Mat. Fys. Medd. **15**, 1 (1937).

[7] J. A. Shercliff, Math. Proc. Cam. Phi. Soc. **49**, 136 (1953).

[8] U. Muller and L. Buhler, *Magnetofluiddynamics in Channels and Containers* (Springer, Berlin, 2001).

[9] P. A. Gilman and E. R. Benton, Phys. Fluids **11**, 2397 (1968).

[10] D. J. Acheson and R. Hide, Rep. Prog. Phys. **36**, 159 (1973).

[11] G. Siráň, Stud. Geophys. Geod. **18**, 248 (1974).

[12] J. Szklarski and G. Rüdiger, Phys. Rev. E **76**, 066308 (2007).

[13] A. H. Roach, E. J. Spence, C. Gissinger, E. M. Edlund, P. Sloboda, J. Goodman, and H. Ji, Phys. Rev. Lett. **108**, 154502 (2012).

[14] E. J. Spence, A. H. Roach, E. M. Edlund, P. Sloboda, and H. Ji, Phys. Plasmas **19**, 056502 (2012).

[15] S. Balbus and J. Hawley, Rev. Mod. Phys. **70**, 1 (1998).

[16] D. R. Sisan, N. Mujica, W. A. Tillotson, Y. M. Huang, W. Dorland, A. B. Hassam, T. M. Antonsen, and D. P. Lathrop, Phys. Rev. Lett. **93**, 114502 (2004).

[17] C. Gissinger, H. Ji, and J. Goodman, Phys. Rev. E **84**, 026308 (2011).

[18] C. Gissinger, J. Goodman, and H. Ji, Phys. Fluids **24**, 074109 (2012).

[19] X. Wei, H. Ji, J. Goodman, F. Ebrahimi, E. Gilson, F. Jenko, and K. Lackner, Phys. Rev. E **94**, 063107 (2016).

[20] D. Brito, H.-C. Nataf, P. Cardin, J. Aubert, and J.-P. Masson, Exp. Fluids **31**, 653 (2001).

[21] J.-L. Guermond, R. Laguerre, J. Léorat, and C. Nore, J. Comp. Phys. **228**, 2739 (2009).

[22] A. Miura and J. R. Kan, Geophys. Res. Lett. **19**, 1611 (1992).

[23] http://arks.princeton.edu/ark:/88435/dsp01x920g025r